










**Raman spectroscopy polarization dependence analysis in two-dimensional gallium sulfide**R. S. Alencar <sup>1,2,3,\*</sup>,† R. Longuinhas <sup>4,\*</sup>,‡ C. Rabelo <sup>2</sup> H. Miranda <sup>5</sup> B. C. Viana <sup>6</sup> A. G. Souza Filho <sup>3</sup>  
L. G. Cançado <sup>2</sup> A. Jorio <sup>2</sup> and J. Ribeiro-Soares <sup>4,§</sup><sup>1</sup>*Faculdade de Física, Universidade Federal do Pará, Belém, Pará 66075-110, Brazil*<sup>2</sup>*Departamento de Física, Universidade Federal de Minas Gerais, Belo Horizonte, Minas Gerais 30270-901, Brazil*<sup>3</sup>*Departamento de Física, Centro de Ciências, Universidade Federal do Ceará, Fortaleza, Ceará 60455-900, Brazil*<sup>4</sup>*Departamento de Física, Universidade Federal de Lavras, Lavras, Minas Gerais 37200-000, Brazil*<sup>5</sup>*Programa de Pós-Graduação em Engenharia Elétrica, Universidade Federal de Minas Gerais, Av. Antônio Carlos 6627, Belo Horizonte, Minas Gerais 31270-901, Brazil*<sup>6</sup>*Departamento de Física, Universidade Federal do Piauí, Teresina, Piauí 64049-550, Brazil*

(Received 21 April 2020; revised 25 July 2020; accepted 3 September 2020; published 16 October 2020)

Group-III post-transition-metal monochalcogenides like gallium sulfide (GaS) are layered semiconductors with weakly interacting adjacent layers, which allow them to be reduced to the two-dimensional nanometric thickness level by different exfoliation approaches, similar to graphene. Here, we investigate the intensity polarization dependence of the Raman modes for a different number of GaS layers and use symmetry analysis and density-functional perturbation theory to provide further information on these structures. The Raman polarization-dependent behaviors of the bulk relative modes  $A_{1g}$  and  $E_{2g}$  were found to be independent of the number of layers, being proportional to  $\cos^2(\theta)$  for  $A_{1g}$  modes and constant for  $E_{2g}$  modes. The computational calculations for two and three layers show Raman active modes emerging at Raman shifts near the bulk Raman modes, with  $A_{1g}$  ( $A_1'$ ) and  $E_g$  ( $E'$ ) symmetries for an even (odd) number of layers, some of them being observed as “shoulders” in the experimental Raman spectra. These phonon modes present Raman tensors with components similar to those observed in bulk, thus explaining the same polar dependencies for different GaS thicknesses. The Raman intensity calculations were made by implementing the specific experimental geometry used here, thus resulting in good qualitative agreement. These results are fundamental for the understanding of the structural and vibrational changes when GaS is reduced to the few-layer limit, layer-number differentiation, and for further symmetry-lowering studies by strain manipulation or substrate interaction, which are routine issues in both fundamental research and device fabrication.

DOI: [10.1103/PhysRevB.102.165307](https://doi.org/10.1103/PhysRevB.102.165307)**I. INTRODUCTION**

The experimental isolation of graphene in 2004 and the subsequent exploitation of phenomena emerging from its reduced dimensionality [1] motivated efforts to study the properties of other two-dimensional (2D) materials, which were also expected to be obtained from layered van der Waals solids well-known in the literature [2–4]. Representative families of these 2D materials are transition-metal dichalcogenides (TMDCs) such as  $\text{MoS}_2$ ,  $\text{WS}_2$ , phosphorene systems and, more recently, post-transition-metal monochalcogenides like GaSe, GaS, InSe, among others [3–5]. These materials are seen as building blocks to fabricate ultimate heterostructures and complement graphene in applications at the nanoscale, thus presenting a myriad of mechanical, optical, electrical, and thermal properties [3–6].

Group-III post-transition-metal monochalcogenides with  $MX$  formula ( $M = \text{Ga}$  or  $\text{In}$ , and  $X = \text{S}$ ,  $\text{Se}$ , or  $\text{Te}$ , see

Fig. 1) have attracted increasing attention due to their specific electronic, optical, and optoelectronic properties, which are promising for high-performance devices, for example [5, 7–10]. On the contrary to TMDCs, in which an indirect-to-direct band-gap transition occurs when the number of layers is progressively reduced to the monolayer level, InSe exhibit a direct-to-indirect band-gap transition from bulk (1.26 eV) to few layer (1.45 eV), thus experiencing different photoluminescence performance as compared to other TMDCs [5]. In multilayer GaSe samples, it was experimentally shown that uniaxial strain redshifts its photoluminescence by approximately 50 meV for a 3% strain level [11]. It was theoretically suggested that GaSe is as good as or even a better lubricant than graphite [12], and also that its monolayer is promising for strain sensing in fragile applications [13]. Bulk GaS possesses an indirect band gap of 3.05 eV [14], being specially promising for near-blue light emitting devices. This band gap is also predicted to be tuned with the increasing thickness from monolayer to bulk, and with mechanical deformations [15], thus making this material particularly interesting for completing the TMDCs in the wide band-gap limit.

Raman spectroscopy has become an important tool for characterizing 2D layered materials (LMs) thanks to the sensitivity of Raman scattering to structural, optical, electronic, and

\*These authors contributed equally to this work.

†rsalencar@ufpa.br

‡raphael.lobato@ufba.br

§jenaina.soares@ufba.br

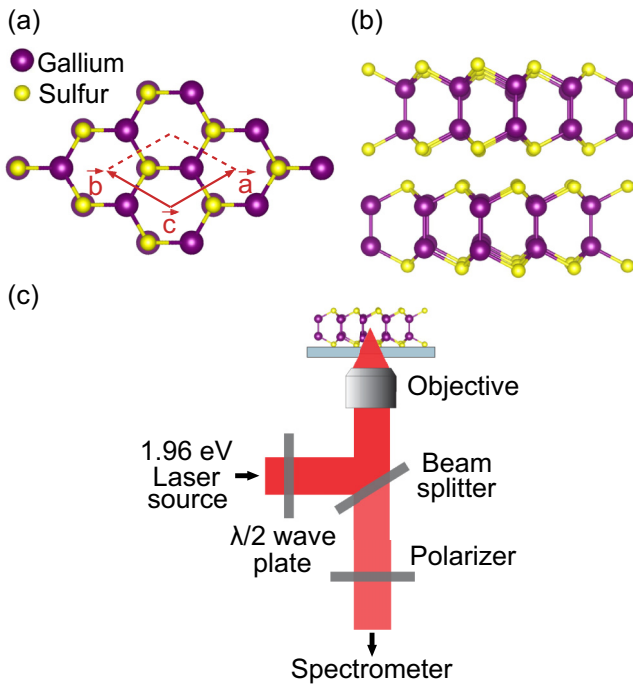


FIG. 1. Bulk gallium sulfide (GaS) lattice structure for the only naturally occurring  $\beta$  polytype [32]. (a) Top view. (b) Side view. When exfoliated, few or even monolayer GaS can be obtained due to the weak van der Waals interactions among adjacent layers. (c) Backscattering experimental geometry used in this paper for acquiring Raman spectra.

chemical properties of this class of materials. Raman spectroscopy has been useful for probing defects [16–18], strain [13,19], LM-substrate adhesion [20,21], doping [22], thermal properties [6,23–27], number of layers [14] and symmetry [12,28–31]. The Raman spectrum of bulk GaS was previously studied in literature [32,33], as well as its temperature dependence [34,35], but only recently its thickness dependence started to be explored in detail [35]. Although ready-to-use analytical functions relating the position of the so-called  $A_{1g}^1$  and  $A_{1g}^2$  modes (190 and 360  $\text{cm}^{-1}$ , respectively) to sample thickness were established [35], their polar dependencies, as well as possible changes induced by the reduced dimensionality, are still open to be addressed.

In this paper, the polar dependencies of the Raman spectra intensities of the various phonon modes of few-layer GaS, as well as their full width at half maximum (FWHM), are measured. Density-functional-perturbation theory methods are used to predict the development of their Raman shifts, and symmetry analysis is performed to access the structural changes when GaS is reduced to a few-layer limit. The decreased dimensionality induced by the exfoliation process and symmetries according to an even or odd number of layers are shown to result in phonon modes with Raman shifts close to known bulk Raman modes, which are used to explain the polar dependencies observed in the intensity versus  $\theta$  plots. The results presented here are valuable to understand the structure of GaS at the few-layer regime, to define the number of layers, as well as the broadening of these phonon modes, and for other works studying their degree of interaction with substrates.

## II. METHODOLOGY

### A. Sample and experimental setup

Few-layer GaS was obtained by standard mechanical exfoliation [36] from a single crystal source provided by 2D Semiconductors and deposited on thin glass coverslips. This step was taken to avoid misinterpretation of one of the significant GaS Raman peaks with the conventionally used silicon substrate, which exhibits a higher-order Raman peak with a complex line shape [7,11,14,37,38] near 303  $\text{cm}^{-1}$ . The sample thicknesses were estimated by optical contrast, Raman spectroscopy, and atomic force microscopy (AFM). The AFM analysis was carried out in ambient conditions using an Asylum Research scanning probe microscope operating in the tapping mode.

Raman experiments were performed using a homebuilt confocal optical microscope system based on an Andor Shamrock SR-303i-A spectrometer, an iDus DU401A-BR-DD CCD, and an inverted Nikon Eclipse Ti-U microscope in a confocal backscattering configuration. A laser energy of 1.96 eV was used to excite the Raman spectra. The laser power was set to 360  $\mu\text{W}$  to improve the signal-to-noise ratio while also avoiding sample damage. The laser beam was focused by a 60 $\times$  oil immersion objective lens of 1.4 numerical aperture (NA) and the signal was dispersed by a 1200 grooves/mm grating, resulting in a spectral resolution of  $\pm 1.4 \text{ cm}^{-1}$ . The influence of the high NA in preserving the light polarization was checked by using NA = 0.25, 2.54 eV excitation energy and grating of 1800 grooves/mm in bulk GaS, and no significant difference generated by the smaller NA was observed, see Fig. S1 of the Supplemental Material (SM) [39].

The polarized Raman experiments were performed by rotating the linearly polarized incident laser beam through a half-wave plate and the scattered light was analyzed by a linear polarizer [see Fig. 1(c)]. The spectrometer's grating and beam-splitter dependencies on polarization were compensated by normalizing the GaS peak intensities by an efficiency function (EF), which was previously defined in the laboratory for the graphene's G band. This EF was defined in such a way that the G band intensity is independent of the incident polarization [40], since this phonon mode belongs to the  $E_{2g}$  irreducible representation [41]. The EF is well defined in the SM [39].

### B. Computational methods

First-principles calculations were performed using density-functional theory (DFT) [42,43] and density-functional-perturbation theory (DFPT) [44] as implemented in the PLANE-WAVE SELF-CONSISTENT FIELD (PWSCF) and PHONON packages of the QUANTUM ESPRESSO distribution [45]. The Brillouin zone integrations were performed within Monkhorst-Pack scheme [46] using  $8 \times 8 \times 4$  and  $8 \times 8 \times 1$   $\Gamma$ -centered grids for the bulk and few-layers GaS. For lattice and atomic position optimizations, the convergence was achieved for forces and stress lower than 0.1 mRy/bohr and 50 MPa, respectively. In the case of the slab models, images are separated by approximately 16  $\text{\AA}$  of vacuum. The exchange-correlation energy is evaluated within local density approximation, using Perdew-Zunger's parametrization

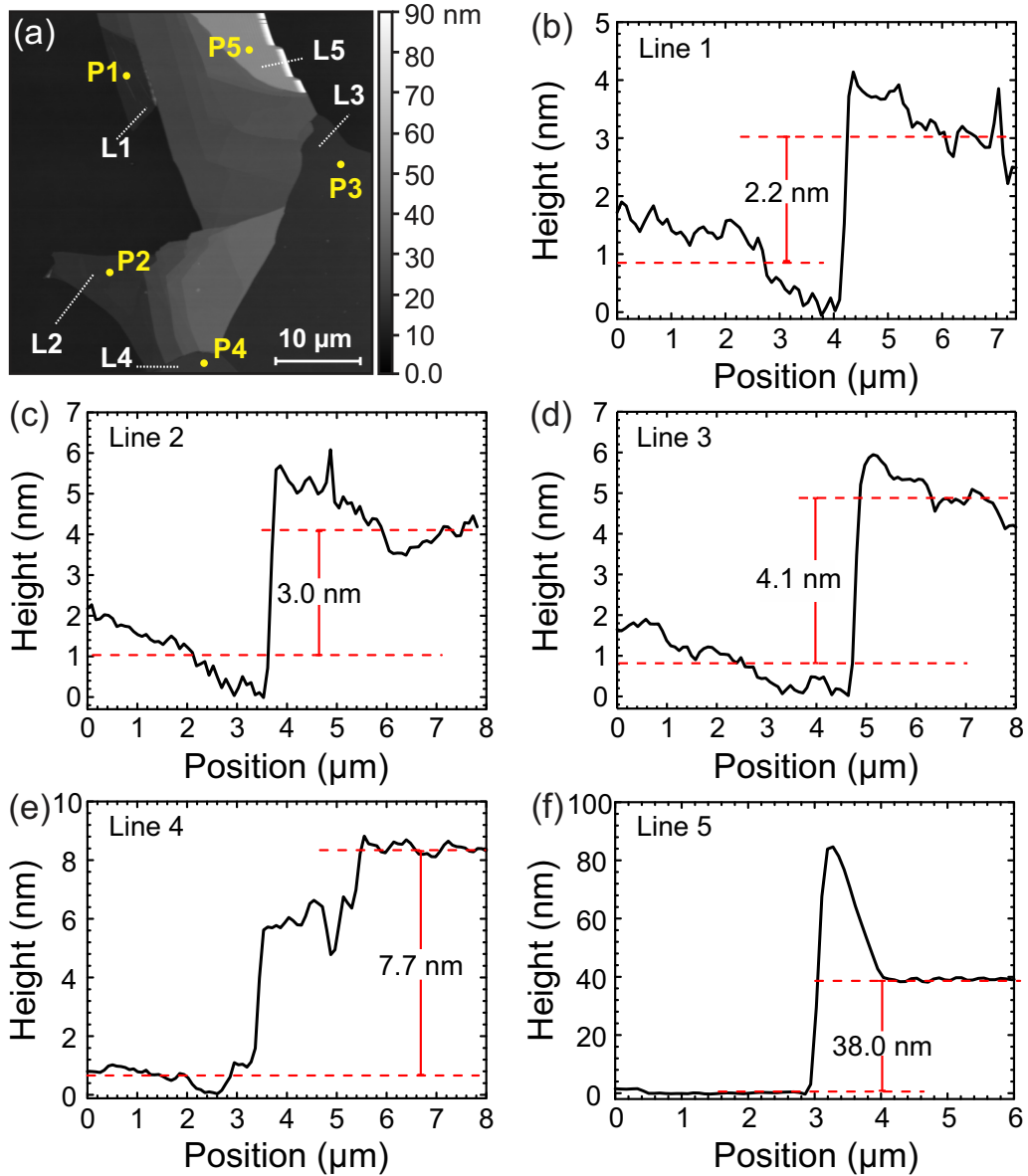


FIG. 2. (a) AFM topographic image from a GaS flake. (b)–(f) Height profiles of five regions acquired along the dashed lines. The yellow dots label the positions where the polarized Raman spectra were carried out.

[47]. The electron-ion interactions were described using a modified Bachelet-Hamann-Schulter [48,49] scheme for norm-conserving pseudopotentials. The plane-wave kinetic energy cutoff to describe the electronic wave functions (charge density) was set to 60 Ry (240 Ry). The phonon Raman shifts and non-resonant Stokes Raman spectra were computed using DFPT [44,50,51]. Gaussian functions were used to provide the visual effect of broadening of the phonon modes for the simulated Raman spectra.

### III. RESULTS AND DISCUSSION

An AFM topographic image of a specified GaS flake with different thicknesses is shown in Fig. 2(a). Thicknesses of five regions, marked by dashed lines, were estimated through height profiles. These regions have thicknesses of 2.2 nm, 3.0 nm, 4.1 nm, 7.7 nm, and 38.0 nm, respectively.

The Raman spectrum of bulk GaS is characterized by five normal modes with the following Raman shifts (irreducible representations):  $22.8 \text{ cm}^{-1}$  ( $E_{2g}^2$ ),  $74.7 \text{ cm}^{-1}$  ( $E_{1g}^1$ ),  $189 \text{ cm}^{-1}$  ( $A_{1g}^1$ ),  $291.8 \text{ cm}^{-1}$  ( $E_{1g}^2$ ),  $295.8 \text{ cm}^{-1}$  ( $E_{2g}^1$ ), and  $360.9 \text{ cm}^{-1}$  ( $A_{1g}^2$ ) [34,52]. Due to the experimental limitations imposed by the long-pass edge filter in the present experimental setup for low Raman shifts, our Raman data analysis is restricted to the modes  $A_{1g}^1$ ,  $E_{2g}^1$ , and  $A_{1g}^2$ . The analysis of the  $E_{1g}^2$  mode is difficult since its Raman shift is close to the  $E_{2g}^1$  mode's and presents smaller intensity [53], especially when the GaS thickness is reduced. Also, both  $E_{1g}^1$  and  $E_{1g}^2$  modes are not allowed in the present backscattering geometry, as will be discussed. The intensities of the  $A_{1g}^1$  and  $A_{1g}^2$  modes decrease considerably as the number of layers decreases [35]. We minimize this problem using a high numerical aperture objective lens, increasing the laser

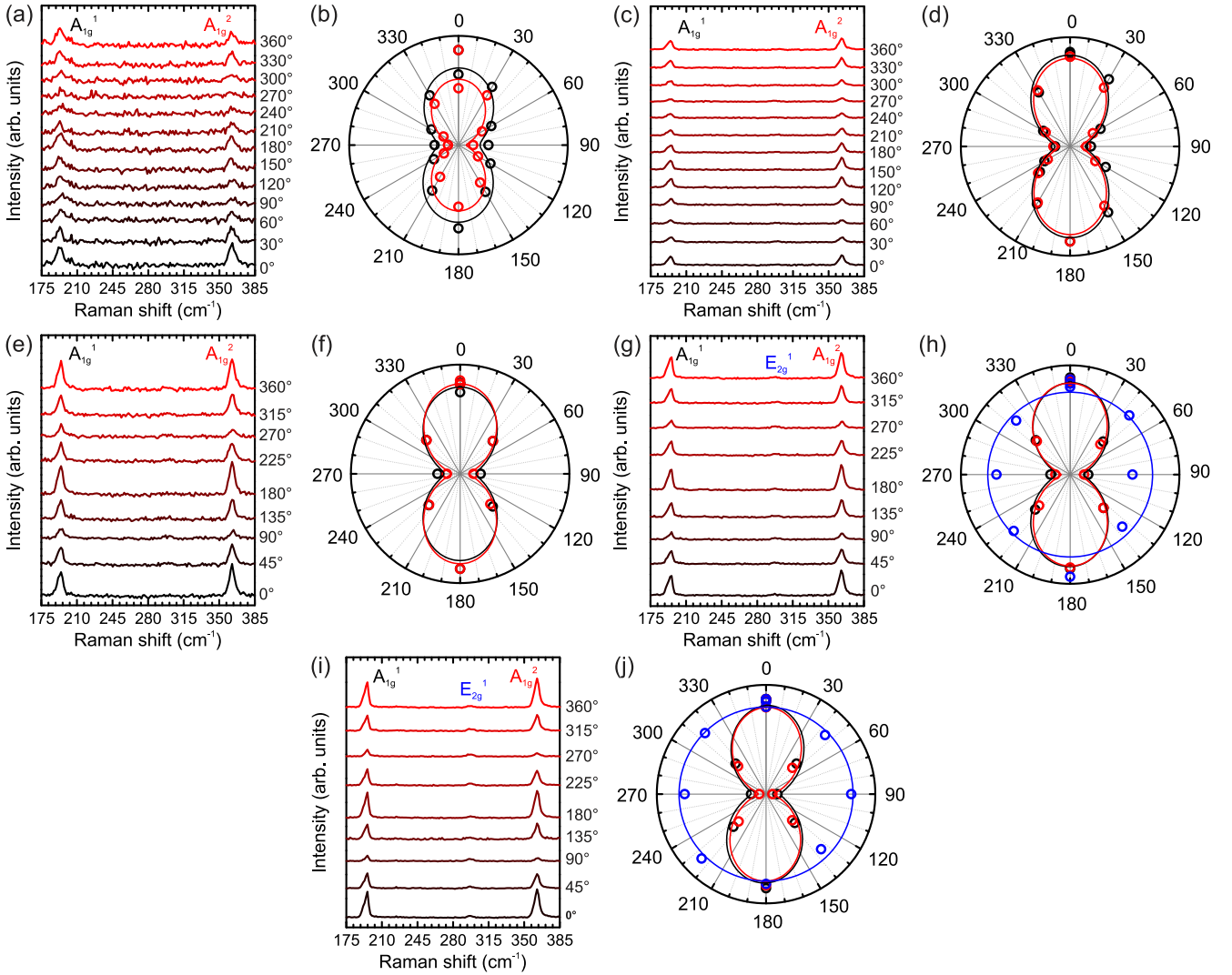


FIG. 3. (a), (c), (e), (g), and (i) are normalized Raman spectra acquired with different polarization angles at the positions P1-P5, respectively. (b), (d), (f), (h), and (j) are polar plots of  $A_{1g}^1$ ,  $E_{2g}^1$ , and  $A_{1g}^2$  modes recorded at the respective positions. Black, blue, and red circles are experimental data from  $A_{1g}^1$ ,  $E_{2g}^1$ , and  $A_{1g}^2$  modes, respectively. The phonon modes irreducible representations superscripts are given here according to the traditional convention used for bulk GaS.

power and the acquisition time to improve the signal-to-noise ratio.

Figures 3(a), 3(c), 3(e), 3(g) and 3(i) show polarized Raman spectra of GaS collected at the positions P1-P5, respectively, as specified in Fig. 2(a). It is worth mentioning that the baselines from the Raman spectra presented here were previously subtracted. For now, we will assume the mode-symmetry assignment attributed to bulk GaS as a label for the corresponding phonon modes in both bulk and few-layer samples. Later on, during the discussion of the experimental results, we will present the correct assignment considering few-layer systems. According to the bulk's nomenclature, the intensities of the Raman modes  $A_{1g}^1$ ,  $E_{2g}^1$ , and  $A_{1g}^2$  decrease with the decreasing of GaS thickness. Furthermore, for a GaS flake with thickness below 7.7 nm, the  $E_{2g}^1$  Raman mode is observed in a couple of spectra and its intensity is not strong enough to allow for solid conclusions. Thus, for positions P1, P2, and P3, we focus only on  $A_{1g}$  modes.

For a more accurate analysis, line-shape analysis for each Raman mode was performed by using one Lorentzian component. The central Raman shifts ( $\omega$ ) and the FWHM ( $\Gamma$ ), for spectra recorded with incident and scattered light vertical polarization ( $0^\circ$ ), are shown in Table I. The  $\omega_{A_{1g}^1}$  downshifts with decreasing thickness, while the  $\omega_{A_{1g}^2}$  value is constant within the uncertainty. On the other hand, the  $\Gamma$  increases for both modes. Actually, the  $\omega_{A_{1g}^1}$  and its  $\Gamma$  have been used to probe the GaS thickness [14,35]. Our findings show an  $A_{1g}^1$  Raman shift difference of  $2.4 \pm 0.3 \text{ cm}^{-1}$  and an increase in  $\Gamma$  of  $3.0 \pm 0.8 \text{ cm}^{-1}$ , when P1 and P5 spectra are compared to each other. According to Ref. [35], the P1 spectrum refers to bilayer GaS, given that the monolayer occurrence was considered for height profiles lower than 1.5 nm, and that 0.7 nm steps in adjacent areas are consistent with GaS single-layer thickness. These results are in agreement with the AFM height profiles from Figs. 2(b) and 2(c). The numbers of layers for P1-P5

TABLE I. Central Raman shifts ( $\omega$ ) and FWHM ( $\Gamma$ ) for the three modes  $A_{1g}^1$ ,  $E_{2g}^1$ , and  $A_{1g}^2$ , considering the bulk counterpart irreducible representation assignment, at the different positions P1–P5 indicated in Fig. 2(a). Spectra are recorded with incident and scattered light vertical polarization ( $0^\circ$ ). The spectral resolution is of  $\pm 1.4 \text{ cm}^{-1}$ .

Position	Thickness (nm)	$A_{1g}^1$ ( $\text{cm}^{-1}$ )		$E_{2g}^1$ ( $\text{cm}^{-1}$ )		$A_{1g}^2$ ( $\text{cm}^{-1}$ )	
		$\omega$	$\Gamma$	$\omega$	$\Gamma$	$\omega$	$\Gamma$
P1	2.2	$187.6 \pm 0.3$	$7.9 \pm 0.6$	...	...	$360.0 \pm 0.2$	$7.7 \pm 0.4$
P2	3.0	$188.0 \pm 0.1$	$5.5 \pm 0.1$	...	...	$360.7 \pm 0.1$	$5.6 \pm 0.1$
P3	4.1	$187.8 \pm 0.1$	$5.7 \pm 0.1$	...	...	$360.6 \pm 0.1$	$5.8 \pm 0.2$
P4	7.7	$188.5 \pm 0.1$	$5.2 \pm 0.1$	$294.3 \pm 0.2$	$6.3 \pm 0.2$	$360.7 \pm 0.1$	$5.5 \pm 0.1$
P5	38.0	$189.0 \pm 0.1$	$4.2 \pm 0.1$	$293.2 \pm 0.1$	$5.6 \pm 0.2$	$360.4 \pm 0.1$	$5.2 \pm 0.1$

are estimated as follows: P1 = 2 layers; P2 = 3 layers; P3 = 4 layers, P4 = 10 layers, and P5 = 53 layers (considered as bulk here).

The polarization dependence of the Raman intensity is shown in Figs. 3(b), 3(d) 3(f), 3(h), and 3(j) for different thicknesses. The intensities of  $A_{1g}$  modes are maximum when the incident light polarization (relative to polarizer polarization) is set at  $0^\circ$  ( $180^\circ$ ) and minimum for  $90^\circ$  ( $270^\circ$ ). In contrast, the  $E_{2g}^1$  intensity does not depend on polarization. It is noteworthy that angle-dependent Raman intensities are, apparently, thickness independent.

Bulk GaS is known to crystallize only in the so-called  $\beta$  polytype [32], in which the weakly van der Waals-interacting atomic quadrilayers (QLs) S-Ga-Ga-S are stacked perpendicular to the basal plane, as previously shown in Figs. 1(a) and 1(b). In this stacking geometry, the Ga atoms of one layer are on top of S atoms of the adjacent layer. The bulk  $\beta$ -GaS unit cell is composed of two structural formulas ( $Z = 2$ ) encompassing four atoms each, so the material belongs to the centrosymmetric space group  $P6_3/mmc$  ( $D_{6h}^4$  according to the Schoenflies notation, or No. 194 in the International Tables for Crystallography Vol. A [54]).

The exfoliation process in few-layer two-dimensional materials provides symmetry variations due to the loss of translational symmetry perpendicular to the basal plane [29]. In  $\beta$ -GaS, the parity of the number of QL's ( $N$ ) plays an important role, with odd  $N$  belonging to the  $P\bar{6}m2$  ( $D_{3h}^1$ , or No. 187) noncentrosymmetric space group, while even  $N$  belongs to the  $P3m1$  ( $D_{3d}^3$ , or No. 164) centrosymmetric space group [55].

The experimental detection of a given Raman-active mode depends on both crystal and measurement geometries, which dictates its scattering intensity. By using the semiclassical modeling for the first-order Raman effect, it is possible to understand the observed behavior of the experimental data obtained for  $\beta$ -GaS, the possible consequences of symmetry variations according to odd or even  $N$ , and also to perform comparisons with the bulk counterpart. In this perspective, the Raman intensity is given by

$$I_n \propto |\langle e_s | \vec{R}_n | e_i \rangle|^2 / \omega_n, \quad (1)$$

where  $|e_i\rangle$  and  $|e_s\rangle$  are the incident and scattered radiation polarization unitary vectors, respectively,  $\omega_n$  is the Raman shift, and  $\vec{R}_n$  the Raman tensor of the  $n$ th phonon mode [50,56].

For  $\beta$ -GaS with an odd number of layers  $N$ , the Raman tensors are

$$A_1' : \begin{pmatrix} a & 0 & 0 \\ 0 & a & 0 \\ 0 & 0 & b \end{pmatrix},$$

$$E' : \begin{pmatrix} d & 0 & 0 \\ 0 & -d & 0 \\ 0 & 0 & 0 \end{pmatrix}, \quad \begin{pmatrix} 0 & -d & 0 \\ -d & 0 & 0 \\ 0 & 0 & 0 \end{pmatrix},$$

$$E'' : \begin{pmatrix} 0 & 0 & -c \\ 0 & 0 & 0 \\ -c & 0 & 0 \end{pmatrix}, \quad \begin{pmatrix} 0 & 0 & 0 \\ 0 & 0 & c \\ 0 & c & 0 \end{pmatrix}.$$

In the case of an even  $N$ , the appropriate Raman tensors are

$$A_{1g} : \begin{pmatrix} a & 0 & 0 \\ 0 & a & 0 \\ 0 & 0 & b \end{pmatrix},$$

$$E_g : \begin{pmatrix} c & 0 & 0 \\ 0 & -c & d \\ 0 & d & 0 \end{pmatrix}, \quad \begin{pmatrix} 0 & -c & -d \\ -c & 0 & 0 \\ -d & 0 & 0 \end{pmatrix}.$$

For bulk  $\beta$ -GaS, the Raman tensors are

$$A_{1g} : \begin{pmatrix} a & 0 & 0 \\ 0 & a & 0 \\ 0 & 0 & b \end{pmatrix},$$

$$E_{1g} : \begin{pmatrix} 0 & 0 & 0 \\ 0 & 0 & c \\ 0 & c & 0 \end{pmatrix}, \quad \begin{pmatrix} 0 & 0 & -c \\ 0 & 0 & 0 \\ -c & 0 & 0 \end{pmatrix},$$

$$E_{2g} : \begin{pmatrix} d & 0 & 0 \\ 0 & -d & 0 \\ 0 & 0 & 0 \end{pmatrix}, \quad \begin{pmatrix} 0 & -d & 0 \\ -d & 0 & 0 \\ 0 & 0 & 0 \end{pmatrix}.$$

A widely used experimental geometry in the field of layered two-dimensional materials is the backscattering measurement configuration, in which the direction of the incident and scattered light propagation are both along the stacking direction  $c = z$ , with opposite sense, as shown in Fig. 1(c). In this situation, the incident and scattered light polarization directions  $|e_i\rangle$  and  $|e_s\rangle$  are in the  $\beta$ -GaS  $xy$  isotropic basal plane. If it is chosen to keep the crystal with its position fixed, the incident light polarization direction  $|e_i\rangle$  can be described as  $|e_i\rangle = |\cos \theta_i, \sin \theta_i, 0\rangle$ , where  $\theta_i$  is the polarization angle relative to the sample axis. The scattered light polarization direction can be described as  $|e_s\rangle = |\cos \theta_s, \sin \theta_s, 0\rangle$ , where

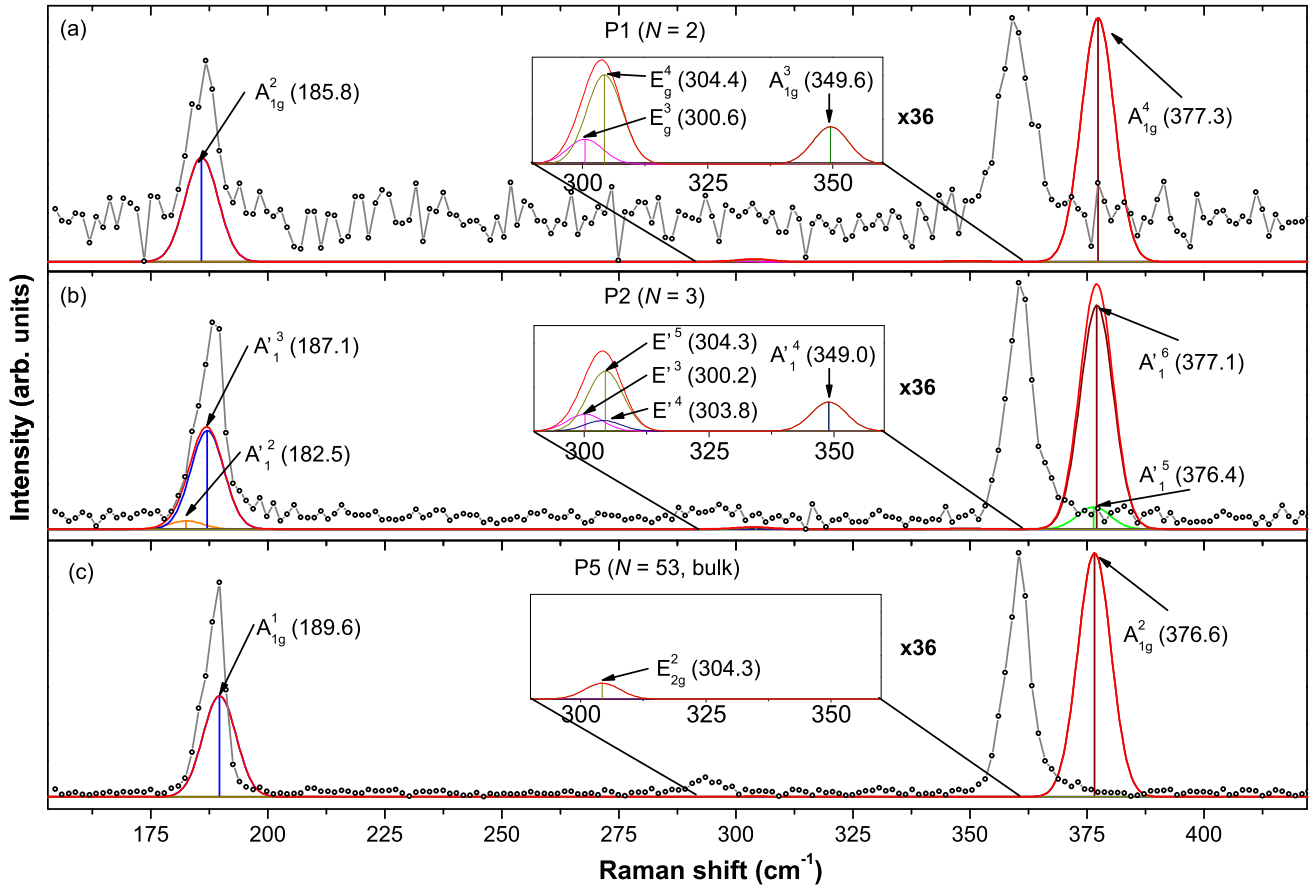


FIG. 4. Experimental (dots + lines) and theoretical (continuous lines) Raman spectra of  $\beta$ -GaS, for points P1 ( $N = 2$ , bilayer), P2 ( $N = 3$ , trilayer), and P5 (53 layers, considered here as bulk). The Raman shifts and intensities for the parallel-polarized theoretical spectra were extracted from DFT calculations, with the red continuous line representing the calculations from Eq. (2) ( $I^{XX}$ ). The Raman shifts and irreducible representations for the phonon modes in the  $I^{XX}$  calculated spectra are indicated.

$\theta_s$  is the polarization angle of the linear polarizer also relative to the sample axis. Due to the in-plane isotropy, we may choose  $\theta_i = \theta$  and let  $\theta_s = 0$  from now on.

In the backscattering geometry, only the Raman-active modes of  $\beta$ -GaS with irreducible representations associated with quadratic basis functions involving  $x$  and  $y$  ( $xx, yy, xy, x^2 - y^2, \dots$ ) will be accessible [41]. Therefore, considering the Raman tensors described above, for odd  $N$  the detection of  $A'_1$  and  $E'$  modes is expected, with the intensities given by  $I(A'_1) \propto a^2 \cos^2(\theta)$  and  $I(E') \propto d^2$ , respectively. For even  $N$ , the  $A_{1g}$  and  $E_g$  modes are accessible, with intensities  $I(A_{1g}) \propto a^2 \cos^2(\theta)$  and  $I(E_g) \propto c^2$  and, for the bulk counterpart, the  $A_{1g}$  and  $E_{2g}$  can be detected, with intensities  $I(A_{1g}) \propto a^2 \cos^2(\theta)$  and  $I(E_{2g}) \propto d^2$ . It is possible to observe that the accessible modes are divided in two types:  $A$  nondegenerate and  $E$  doubly degenerate Raman-active modes. This occurs because the exfoliation process preserves the in-layer symmetry, being the spacial groups for  $N$  odd and  $N$  even number of layers high-symmetry subgroups from the bulk  $\beta$ -GaS space group. Our results show that these modes exhibits similar polar-dependent behavior within the same type, irrespective of the number of layers.

To gather further information about the lattice dynamics, we simulated the lattice vibrations in NL-GaS, for  $N = 2$ ,  $N = 3$ , and bulk (represented here by the thickest sample

in P5). By using the simulation parameters detailed in the Methodology section, we found the in-plane lattice constants of 2L, 3L, and bulk to be equal to 3.499, 3.500, and 3.502 Å, respectively, and the out-of-plane lattice parameter for bulk equal to 15.083 Å, in excellent agreement with available experimental data for bulk, where  $a = 3.587(3)$  and  $c = 15.492(7)$  [57]. We calculate the intensity of the parallel-polarized, non-resonant Raman spectra by using [58]

$$I_n^{XX} \propto |\langle \hat{x} | \vec{R}_n | \hat{x} \rangle|^2 / \omega_n. \quad (2)$$

The use of Eq. (2) is justified by the following reasons: (i) we do not have powder GaS, but single crystals with in-plane isotropy instead and (ii) the experimental data were acquired in the parallel  $XX$  backscattering geometry, with angle 0 among the incident and scattered light polarization in the  $X$  direction, corresponding to the maximum intensities of the  $A$ -type modes. The comparison of the intensities calculated from Eq. (2) ( $I^{XX}$ ) and the experimental data is shown in Fig. 4. The relative intensity of the  $A_{1g}$  modes in bulk GaS,  $I_{A_{1g}^2} / I_{A_{1g}^1}$ , is greater than unity in both experiments and results from Eq. (2), reaching overall good qualitative agreement. However, it is important to note that the theoretical relative intensity of the out-of-plane modes can be sensitive to the thickness of the slab used in calculations, due to the fact

that the out-of-plane components of the polarizability and its derivatives to out-of-plane atomic motion are ill defined in this case [58]. The analysis of this subject is beyond the scope of the present paper.

The simulated Raman spectra, mode Raman shifts, and irreducible representations for the phonon modes accessible in the  $XX$  parallel backscattering configuration are shown in Fig. 4. The superscripts of the irreducible representations are given in increasing order, from lower to higher Raman shift. As such, the  $E_{2g}^1$  mode near  $295.8 \text{ cm}^{-1}$ , in the bulk nomenclature previously shown, is renamed here  $E_{2g}^2$ , since the low-frequency interlayer mode near  $22.8 \text{ cm}^{-1}$  is not experimentally accessible here (but reported in Ref. [33] at  $22 \text{ cm}^{-1}$ ). The overlap of the nonpolarized experimental Raman data and calculated spectra is also displayed, and a normalization to the intensity of the  $A$ -type nondegenerate mode with the highest peak position center was performed. By taking the experimental Raman shifts of the most intense peaks as a reference, and comparing to the most intense calculated peaks, the relative errors were of 0.32% ( $A_{1g}^2$ ) and 4.92% ( $A_{1g}^4$ ) in P1, 0.53% ( $A_1^3$ ), and 4.55% ( $A_1^6$ ) in P2, and 0.42% ( $A_{1g}^1$ ), 3.64% ( $E_{2g}^2$ ), and 4.50% ( $A_{1g}^2$ ) in P5, which are reasonable.

The simulated spectra show that new additional phonon modes of GaS appear in the few-layer limit. The new modes are  $A_{1g}$  and  $E_g$  for P1 with  $N = 2$ , and  $A_1'$  and  $E'$  for P2 with  $N = 3$ , from the  $A$  nondegenerate and  $E$  doubly degenerate types. The superscripts of these irreducible representations are also given in increasing order, being  $A_{1g}^1, E_g^1$ , and  $E_g^2$  for  $N = 2$ , and  $A_1^1, E^1$ , and  $E^2$  for  $N = 3$ , not accessible in this experimental range. It is important to note that, in P1, the  $E_g^3$  and  $A_{1g}^3$  additional modes arise, while in P2, the  $A_1^2, E^3, E^4, A_1^4$ , and  $A_1^5$ , new modes emerge, P1 and P2 being in the thinner regions measured. The P2 experimental data shows the emergence of a left “shoulder” for the peak near the predicted  $A_1^2$  ( $182.5 \text{ cm}^{-1}$ ) and  $A_1^3$  ( $187.1 \text{ cm}^{-1}$ ) modes, as well as for the right shoulder for the peak near  $A_1^5$  ( $376.4 \text{ cm}^{-1}$ ) and  $A_1^6$  ( $377.1 \text{ cm}^{-1}$ ), see Fig. S3 of the SM [39]. This indicates that the new modes are present and contribute for the general intensity, which can be used as a strategy to distinguish  $N = 2$  and  $N = 3$  in future Raman studies with higher spectral resolution and better signal-to-noise ratio. The explanation for this result can be based on the fact that the translational symmetry along the stacking axis is lost in the exfoliation process and the unit cells possesses an increasing number of atoms with the increase of the number of GaS layers, contrary to the unit cell of the bulk counterpart, thus resulting in the observation of new modes.

The new modes are expected to display their polar intensity dependencies in the case of polarization-dependent Raman studies, which could impact the results shown here. It can be observed that the new modes appearing in the vicinity of the  $A_{1g}$  and  $E_{2g}$  bulk modes are also of  $A$  nondegenerate and  $E$  doubly degenerate Raman-active modes which, as commented before, have the same polar dependence as observed for the modes in the bulk sample. For this reason, the peaks composed by more than one phonon mode display the same behavior as expected for the modes in their bulk counterpart in the same Raman shift region.

The occurrence of new modes in the few-layer limit can lead to the expectation of peak broadening, in agreement with our experimental results (see Table I), thus corroborating previous studies [14,35,59]. It was recently found that the phonon correlation lengths for the  $A_{1g}^1$  and  $A_{1g}^2$  modes of GaS increase with increasing the number of layers, which is attributed to the progressive decrease of scattering due to surface roughness [59]. As formerly studied for other layered nanomaterials [16–18], the increasing amount of defects leads to the broadening of characteristic Raman bands. Thus, scattering with surface roughness and defects can also increase the FWHM of both  $A_{1g}$  modes. However, this point is beyond the goal of the present paper and requires further investigation.

#### IV. CONCLUSIONS

In summary, we have used experimental and theoretical approaches for addressing the polar dependence of the intensity of Raman modes of few-layer GaS. The exfoliation process was found to break the translational symmetry along the direction perpendicular to the basal plane of GaS layers, giving rise to different space groups for an odd or even number of layers. As a consequence, the  $D_{6h}^4$  GaS bulk space group is changed to the  $D_{3h}^1$  space group for an odd number of layers, and  $D_{3d}^3$  when the number of layers is even. Although the bulk GaS modes, usually observed at  $189 \text{ cm}^{-1}$  ( $A_{1g}^1$ ),  $295.8 \text{ cm}^{-1}$  ( $E_{2g}^1$ ), and  $360.9 \text{ cm}^{-1}$  ( $A_{1g}^2$ ) [34,52], are used to identify the modes in few-layer GaS, it was shown here by DFPT calculations for two and three layers that new Raman active modes are activated in these systems due to the reduced reduced dimensionality. These modes, appearing at the vicinity of the bulk Raman modes, belong to  $A_{1g}$  and  $E_g$  symmetries for an even number of layers and  $A_1'$  and  $E'$  for an odd number of layers, with experimental evidence appearing as shoulders in the Raman spectra from new  $A_1'$  modes for a number of layers  $N = 3$ . The polarization dependence of the studied Raman spectra does not change noticeably with number of layers. This agrees with the symmetry analysis of the tensors for the new Raman active modes observed for these few layers, which are similar to those of the bulk GaS counterpart. An adapted intensity calculation formula for the DFPT calculations was introduced, considering the backscattering geometry used in this paper, presenting good qualitative agreement with the experimental results. The results presented here are valuable to understand the fundamental structure of exfoliated GaS, as well as in studies relating Raman shift and FWHM changes due to substrate interaction or strain, for example, which are relevant effects for device engineering and further developments. The approach presented here is suitable to analyze the Raman behavior of similar isostructural thin materials.

#### ACKNOWLEDGMENTS

The authors acknowledge financial support from the National Council for Scientific and Technological Development (CNPq/Brazil Grants No. 400397/2014-5, No. 153532/2016-5, No. 150379/2017-0, No. 309309/2017-4, No. 310813/2017-4, No. 427084/2018-0, No. 433027/2018-5, No. 302775/2018-8, No. 420364/2018-8, No.

307901/2019-0, No. 442577/2019-2, and No. 442521/2019-7), from the National Council for the Improvement of Higher Education (CAPES/Brazil Grants RELAI, No. 88881.198744/2018-01 and No. 88887.162565/2018-00 and Procad 88881.068457/2014-01), from the Foundation for Research Support of Minas Gerais (FAPEMIG/Brazil Grants No. TEC-AUC-00026-16, No. RED-00185-16, No. RED-00282-16, No. CEX-APQ-01865-17, and APQ-01980-18), from the Agency for Financing Studies

and Projects (FINEP/Brazil 02/2014 NANO No. 0501/16, 02/2016, and No. 01.13.0330.00) from INCT Nanocarbono and FAPEPI ENERGIAS RENOVÁVEIS 001/2018, and from the Pró-Reitoria de Pesquisa and Pró-Reitoria de Gestão (UFLA) and the prize L'ORÉAL-UNESCO-ABC Prêmio Para Mulheres na Ciência (For Women in Science Prize - Brazil/2017). We also thank the computational time at CENAPAD-SP, CENAPAD-RJ/LNCC, SDumont Supercomputer/LNCC, DFI-UFLA and LCC-UFLA.

- [1] K. S. Novoselov, A. K. Geim, S. V. Morozov, D. Jiang, Y. Zhang, S. V. Dubonos, I. V. Grigorieva, and A. A. Firsov, Electric field effect in atomically thin carbon films, *Science* **306**, 666 (2004).
- [2] M. Chhowalla, H. S. Shin, G. Eda, L.-J. Li, K. P. Loh, and H. Zhang, The chemistry of two-dimensional layered transition metal dichalcogenide nanosheets, *Nat. Chem.* **5**, 263 (2013).
- [3] S. Z. Butler, S. M. Hollen, L. Cao, Y. Cui, J. A. Gupta, H. R. Gutiérrez, T. F. Heinz, S. S. Hong, J. Huang, A. F. Ismach, E. Johnston-Halperin, M. Kuno, V. V. Plashnitsa, R. D. Robinson, R. S. Ruoff, S. Salahuddin, J. Shan, L. Shi, M. G. Spencer, M. Terrones, W. Windl, and J. E. Goldberger, Progress, challenges, and opportunities in two-dimensional materials beyond graphene, *ACS Nano* **7**, 2898 (2013).
- [4] A. C. Ferrari, F. Bonaccorso, V. Fal'Ko, K. S. Novoselov, S. Roche, P. Bøggild, S. Borini, F. H. L. Koppens, V. Palermo, N. Pugno *et al.*, Science and technology roadmap for graphene, related two-dimensional crystals, and hybrid systems, *Nanoscale* **7**, 4598 (2015).
- [5] W. Huang, L. Gan, H. Li, Y. Ma, and T. Zhai, 2D layered group IIIA metal chalcogenides: Synthesis, properties and applications in electronics and optoelectronics, *CrystEngComm* **18**, 3968 (2016).
- [6] T. C. V. Carvalho, F. D. V. Araujo, C. Costa dos Santos, L. M. R. Alencar, J. Ribeiro-Soares, D. J. Late, A. O. Lobo, A. G. Souza Filho, R. S. Alencar, and B. C. Viana, Temperature-dependent phonon dynamics of supported and suspended monolayer tungsten diselenide, *AIP Adv.* **9**, 085316 (2019).
- [7] D. J. Late, B. Liu, J. Luo, A. Yan, H. S. S. Ramakrishna Matte, M. Grayson, C. N. R. Rao, and V. P. Dravid, Gas and GaSe ultrathin layer transistors, *Adv. Mater.* **24**, 3549 (2012).
- [8] V. Zolyomi, N. D. Drummond, and V. I. Fal'Ko, Band structure and optical transitions in atomic layers of hexagonal gallium chalcogenides, *Phys. Rev. B* **87**, 195403 (2013).
- [9] D. J. Terry, V. Zolyomi, M. Hamer, A. V. Tyurnina, D. G. Hopkinson, A. M. Rakowski, S. J. Magorrian, N. Clark, Y. M. Andreev, O. Kazakova *et al.*, Infrared-to-violet tunable optical activity in atomic films of GaSe, InSe, and their heterostructures, *2D Mater.* **5**, 041009 (2018).
- [10] Z. B. Aziza, V. Zolyomi, H. Henck, D. Pierucci, M. G. Silly, J. Avila, S. J. Magorrian, J. Chaste, C. Chen, M. Yoon *et al.*, Valence band inversion and spin-orbit effects in the electronic structure of monolayer GaSe, *Phys. Rev. B* **98**, 115405 (2018).
- [11] C. S. Jung, F. Shojaei, K. Park, J. Y. Oh, H. S. Im, D. M. Jang, J. Park, and H. S. Kang, Red-to-ultraviolet emission tuning of two-dimensional gallium sulfide/selenide, *ACS Nano* **9**, 9585 (2015).
- [12] R. Longuihos and J. Ribeiro-Soares, Ultra-weak interlayer coupling in two-dimensional gallium selenide, *Phys. Chem. Chem. Phys.* **18**, 25401 (2016).
- [13] R. Longuihos and J. Ribeiro-Soares, Monitoring the Applied Strain in Monolayer Gallium Selenide Through Vibrational Spectroscopies: A First-Principles Investigation, *Phys. Rev. Appl.* **11**, 024012 (2019).
- [14] D. J. Late, B. Liu, H. S. S. Ramakrishna Matte, C. N. R. Rao, and V. P. Dravid, Rapid characterization of ultrathin layers of chalcogenides on SiO<sub>2</sub>/Si substrates, *Adv. Funct. Mater.* **22**, 1894 (2012).
- [15] Y. Ma, Y. Dai, M. Guo, L. Yu, and B. Huang, Tunable electronic and dielectric behavior of gas and GaSe monolayers, *Phys. Chem. Chem. Phys.* **15**, 7098 (2013).
- [16] S. Mignuzzi, A. J. Pollard, N. Bonini, B. Brennan, I. S. Gilmore, M. A. Pimenta, D. Richards, and D. Roy, Effect of disorder on Raman scattering of single-layer MoS<sub>2</sub>, *Phys. Rev. B* **91**, 195411 (2015).
- [17] J. Ribeiro-Soares, M. E. Oliveros, C. Garin, M. V. David, L. G. P. Martins, C. A. Almeida, E. H. Martins-Ferreira, K. Takai, T. Enoki, R. Magalhães-Paniago *et al.*, Structural analysis of polycrystalline graphene systems by Raman spectroscopy, *Carbon* **95**, 646 (2015).
- [18] L. G. Cançado, M. G. Da Silva, E. H. M. Ferreira, F. Hof, K. Kampioti, K. Huang, A. Pénicaud, C. A. Achete, R. B. Capaz, and A. Jorio, Disentangling contributions of point and line defects in the Raman spectra of graphene-related materials, *2D Mater.* **4**, 025039 (2017).
- [19] J. Zabel, R. R. Nair, A. Ott, T. Georgiou, A. K. Geim, K. S. Novoselov, and C. Casiraghi, Raman spectroscopy of graphene and bilayer under biaxial strain: Bubbles and balloons, *Nano Lett.* **12**, 617 (2012).
- [20] R. S. Alencar, K. D. A. Saboia, D. Machon, G. Montagnac, V. Meunier, O. P. Ferreira, A. San-Miguel, and A. G. Souza Filho, Atomic-layered MoS<sub>2</sub> on SiO<sub>2</sub> under high pressure: Bimodal adhesion and biaxial strain effects, *Phys. Rev. Mater.* **1**, 024002 (2017).
- [21] D. Machon, C. Bousige, R. Alencar, A. Torres-Dias, F. Balima, J. Nicolle, G. de Sousa Pinheiro, A. G. Souza Filho, and A. San-Miguel, Raman scattering studies of graphene under high pressure, *J. Raman Spectrosc.* **49**, 121 (2018).
- [22] A. Das, S. Pisana, B. Chakraborty, S. Piscanec, S. K. Saha, U. V. Waghmare, K. S. Novoselov, H. R. Krishnamurthy, A. K. Geim, A. C. Ferrari, and A. K. Sood, Monitoring dopants by Raman scattering in an electrochemically top-gated graphene transistor, *Nat. Nanotechnol.* **3**, 210 (2008).



- [23] A. A. Balandin, S. Ghosh, W. Bao, I. Calizo, D. Teweldebrhan, F. Miao, and C. N. Lau, Superior thermal conductivity of single-layer graphene, *Nano Lett.* **8**, 902 (2008).
- [24] D. J. Late, S. N. Shirodkar, U. V. Waghmare, V. P. Dravid, and C. N. R. Rao, Thermal expansion, anharmonicity and temperature-dependent Raman spectra of single- and few-layer *mse2* and *wse2*, *ChemPhysChem* **15**, 1592 (2014).
- [25] D. J. Late *et al.*, Temperature dependent phonon shifts in single-layer *ws* (2), *ACS Appl. Mater. Interfaces* **6**, 1158 (2014).
- [26] D. J. Late, Temperature dependent phonon shifts in few-layer black phosphorus, *ACS Appl. Mater. Interfaces* **7**, 5857 (2015).
- [27] A. G. Vieira, C. Luz-Lima, G. S. Pinheiro, Z. Lin, J. A. Rodríguez-Manzo, N. Perea-López, A. L. Elías, M. Drndić, M. Terrones, H. Terrones *et al.*, Temperature- and power-dependent phonon properties of suspended continuous  $WS_2$  monolayer films, *Vib. Spectrosc.* **86**, 270 (2016).
- [28] Y. Zhao, X. Luo, H. Li, J. Zhang, P. T. Araujo, C. K. Gan, J. Wu, H. Zhang, S. Y. Quek, M. S. Dresselhaus *et al.*, Interlayer breathing and shear modes in few-trilayer  $MoS_2$  and  $WSe_2$ , *Nano Lett.* **13**, 1007 (2013).
- [29] J. Ribeiro-Soares, R. M. Almeida, E. B. Barros, P. T. Araujo, M. S. Dresselhaus, L. G. Cançado, and A. Jorio, Group theory analysis of phonons in two-dimensional transition metal dichalcogenides, *Phys. Rev. B* **90**, 115438 (2014).
- [30] J. Ribeiro-Soares, R. M. Almeida, L. G. Cançado, M. S. Dresselhaus, and A. Jorio, Group theory for structural analysis and lattice vibrations in phosphorene systems, *Phys. Rev. B* **91**, 205421 (2015).
- [31] G. Froehlicher, E. Lorchat, F. Fernique, C. Joshi, A. Molina-Sánchez, L. Wirtz, and S. Berciaud, Unified description of the optical phonon modes in *N*-layer  $MoTe_2$ , *Nano Lett.* **15**, 6481 (2015).
- [32] J. C. Irwin, R. M. Hoff, B. P. Clayman, and R. A. Bromley, Long wavelength lattice vibrations in gas and  $GaSe$ , *Solid State Commun.* **13**, 1531 (1973).
- [33] G. Lucazeau, Vibrational spectra of a gas single crystal, *Solid State Commun.* **18**, 917 (1976).
- [34] N. M. Gasanly, A. Aydınli, H. Özkan, and C. Kocabaş, Temperature dependence of the first-order Raman scattering in gas layered crystals, *Solid State Commun.* **116**, 147 (2000).
- [35] C. Jastrzebski, K. Olkowska, D. J. Jastrzebski, M. Wierzbicki, W. Gebicki, and S. Podsiadlo, Raman scattering studies on very thin layers of gallium sulfide ( $GaS$ ) as a function of sample thickness and temperature, *J. Phys.: Condens. Matter* **31**, 075303 (2019).
- [36] K. S. Novoselov and A. H. Castro Neto, Two-dimensional crystals-based heterostructures: materials with tailored properties, *Phys. Scr.* **T146**, 014006 (2012).
- [37] Y. Lu, J. Chen, T. Chen, Y. Shu, R.-J. Chang, Y. Sheng, V. Shautsova, N. Mkhize, P. Holdway, H. Bhaskaran, and J. H. Warner, Controlling defects in continuous 2D  $GaS$  films for high-performance wavelength-tunable UV-discriminating photodetectors, *Adv. Mater.* **1906958**.
- [38] P. Hu, L. Wang, M. Yoon, J. Zhang, W. Feng, X. Wang, Z. Wen, J. C. Idrobo, Y. Miyamoto, D. B. Geohegan, and K. Xiao, Highly responsive ultrathin gas nanosheet photodetectors on rigid and flexible substrates, *Nano Lett.* **13**, 1649 (2013).
- [39] See Supplemental Material at <http://link.aps.org/supplemental/10.1103/PhysRevB.102.165307> for comprehensive discussions on the experimental methods and additional figures that contribute with the understanding of the paper.
- [40] D. Yoon, H. Moon, Y.-W. Son, G. Samsonidze, B. H. Park, J. B. Kim, Y. P. Lee, and H. Cheong, Strong polarization dependence of double-resonant Raman intensities in graphene, *Nano Lett.* **8**, 4270 (2008).
- [41] A. Jorio, M. S. Dresselhaus, and R. Saito and G. Dresselhaus, *Raman Spectroscopy in Graphene Related Systems*, 1st ed. (Wiley-VCH, Weinheim, Germany, 2011).
- [42] P. Hohenberg and W. Kohn, Inhomogeneous electron gas, *Phys. Rev.* **136**, B864 (1964).
- [43] W. Kohn and L. J. Sham, Self-consistent equations including exchange and correlation effects, *Phys. Rev.* **140**, A1133 (1965).
- [44] S. Baroni, S. de Gironcoli, A. Dal Corso, and P. Giannozzi, Phonons and related crystal properties from density-functional perturbation theory, *Rev. Mod. Phys.* **73**, 515 (2001).
- [45] P. Giannozzi, S. Baroni, N. Bonini, M. Calandra, R. Car, C. Cavazzoni, D. Ceresoli, G. L. Chiarotti, M. Cococcioni, I. Dabo, A. D. Corso, S. de Gironcoli, S. Fabris, G. Fratesi, R. Gebauer, U. Gerstmann, C. Gougoussis, A. Kokalj, M. Lazzeri, L. Martin-Samos, N. Marzari, F. Mauri, R. Mazzarello, S. Paolini, A. Pasquarello, L. Paulatto, C. Sbraccia, S. Scandolo, G. Sclauzero, A. P. Seitsonen, A. Smogunov, P. Umari, and R. M. Wentzcovitch, Quantum ESPRESSO: A modular and open-source software project for quantum simulations of materials, *J. Phys.: Condens. Matter* **21**, 395502 (2009).
- [46] H. J. Monkhorst and J. D. Pack, Special points for Brillouin-zone integrations, *Phys. Rev. B* **13**, 5188 (1976).
- [47] J. P. Perdew and A. Zunger, Self-interaction correction to density-functional approximations for the many-electron systems, *Phys. Rev. B* **23**, 5048 (1981).
- [48] G. B. Bachelet, D. R. Hamann, and M. Schlüter, Pseudopotentials that work: From H to Pu, *Phys. Rev. B* **26**, 4199 (1982).
- [49] X. Gonze, R. Stumpf, and M. Scheffler, Analysis of separable potentials, *Phys. Rev. B* **44**, 8503 (1991).
- [50] M. Lazzeri and F. Mauri, First-Principles Calculation of Vibrational Raman Spectra in Large Systems: Signature of Small Rings in Crystalline  $SiO_2$ , *Phys. Rev. Lett.* **90**, 036401 (2003).
- [51] D. Porezag and M. R. Pederson, Infrared intensities and Raman-scattering activities within density-functional theory, *Phys. Rev. B* **54**, 7830 (1996).
- [52] J. P. van der Ziel, A. E. Meixner, and H. M. Kasper, Raman scattering from  $\beta$ -gas, *Solid State Commun.* **12**, 1213 (1973).
- [53] X. Zhang, Q.-H. Tan, J.-B. Wu, W. Shi, and P.-H. Tan, Review on the Raman spectroscopy of different types of layered materials, *Nanoscale* **8**, 6435 (2016).
- [54] *International Tables for Crystallography*, 5th ed., Space-Group Symmetry, Vol. A, edited by T. Hahn (Springer, Dordrecht, Netherlands, 2005).
- [55] H. Terrones, E. Del Corro, S. Feng, J. M. Poumirol, D. Rhodes, D. Smirnov, N. R. Pradhan, Z. Lin, M. A. T. Nguyen, A. L. Elías, T. E. Mallouk, L. Balicas, M. A. Pimenta, and M. Terrones, New first order Raman-active modes in few layered transition metal dichalcogenides, *Sci. Rep.* **4**, 4215 (2014).

- [56] R. Beams, L. G. Cançado, S. Krylyuk, I. Kalish, B. Kalanyan, A. K. Singh, K. Choudhary, A. Bruma, P. M. Vora, F. Tavazza, A. V. Davydov, and S. J. Stranick, Characterization of few-layer 1T'  $\text{MoTe}_2$  by polarization-resolved second harmonic generation and Raman scattering, *ACS Nano* **10**, 9626 (2016).
- [57] A. Kuhn, A. Chevy, and R. Chevalier, Refinement of the 2h gas  $\beta$ -type, *Acta Cryst. B* **32**, 983 (1976).
- [58] D. Doratotaj, J. R. Simpson, and J.-A. Yan, Probing the uniaxial strains in  $\text{MoS}_2$  using polarized Raman spectroscopy: A first-principles study, *Phys. Rev. B* **93**, 075401 (2016).
- [59] R. S. Alencar, C. Rabelo, H. L. S. Miranda, T. L. Vasconcelos, B. S. Oliveira, A. Ribeiro, B. C. Públio, J. Ribeiro-Soares, A. G. Souza Filho, L. G. Cançado, and A. Jorio, Probing spatial phonon correlation length in post-transition metal monochalcogenide gas using tip-enhanced Raman spectroscopy, *Nano Lett.* **19**, 7357 (2019).